Small-signal modeling of the incremental optical encoder for motor control.

Yeny Vázquez-Gutiérrez, Dara L. O'Sullivan and Richard C. Kavanagh, *Senior Member of IEEE*

***Abstract*— The small-signal model of the incremental optical encoder introduced in this paper provides an insight on the impact of this sensor in the dynamics of the motion control loop of a motor drive. The model is derived and validated for the most commonly employed speed estimation methods: the pulse count and the elapsed time methods. Using the model, the reduction of the phase margin due to the encoder phase lag can be quantified at an early design stage. This model facilitates the design of control techniques to compensate for the phase margin reduction due to the associated feedback delays.**

***Index Terms* — Control design, incremental optical encoder, dynamics, small-signal model, low resolution encoder, low speed, motor drives, motor.**

I. INTRODUCTION

MOTOR drives play a key role in modern industry, with the performance of the intrinsically closed-loop system being greatly determined by the choice of feedback sensor. The present work focuses on square incremental optical encoders and their impact on motor motion control. This sensor is frequently found in applications such as computer numerical control (CNC) machines, printers, paper production, food and beverage automation, elevator control and health assessment of rotating machines [1], etc; where it is principally used for feedback in speed loops.

The output of this sensor is a square signal with frequency nominally proportional to the speed [2]. However, the quantized and sampled position measurement limits the performance of the system [3]. Some of the reported adverse effects are: vibration [3], torque ripples [4] and [5], or motor noise [6]. Specific studies on the field oriented control (FOC) for permanent magnet synchronous motors (PMSM) are found in [5] and [7]. The quantized nature of the sensor can induce limit cycling in the system, causing speed oscillations [8]. Speed oscillation in encoder-based systems is studied in [9] by means of a harmonic approximation. The encoder also reduces the control bandwidth [6], [10], and causes the estimated motor speed to intrinsically lag the actual speed. Various speed estimation methods have been developed to reduce the estimation lag. Those methods are classified in two main types: non-model-based [3],[11]-[12], and model-based methods [13]-[14].

When the number of encoder transitions per control sample time (T_s) is higher than one, the negative effect of the measurement error is more significant than measurement delay to the control-loop performance. The simple solution of low-pass-filtering of the velocity estimate is not favored due to bandwidth reduction, so alternative approaches are provided in [3] and [15] that reduce the phase lag. More advanced techniques are also explored [14], [16] and [17]. These provide an improvement of the noise rejection capabilities, while preserving a good dynamic performance.

When the number of encoder transitions per control sample interval is less than one, the measurement delay can become significant due to the infrequent encoder updating of the position information [18]. Under those circumstances, the frequency response of the motor drive control loop can be impacted by the dynamics of the encoder. The system can even become unstable due to the dynamics of the encoder, if it is not considered when tuning the speed loop compensator. Observers have been employed to provide a model-based state estimation technique when the rate of encoder feedback is low [19]. However, the uncertainty in the plant model or parameters can limit the performance, increase the computational burden [20], or possibly necessitate the application of system identification techniques, [21], [22] to update the motor parameters of the observer.

The small-signal model of the incremental optical encoder facilitates significantly the implementation of simple control techniques like a proportional-integral (PI) or proportional-integral-differential (PID) controllers, at low speed with low resolution devices. An expression for the encoder dynamics (in the form of a delay) is presented in [23] for high speed. The model predicts a unity gain and a phase lag of half of the control sampling interval ($T_s/2$). The same paper proposes a low-speed model with unity gain but time delay equal to the time between consecutive encoder transitions (T_e), for $T_e > T_s$. Also for low speed, a model is derived in [24] as a sample and hold with an average delay of $T_e/2$.

The major contribution of this work is the derivation of

Manuscript received August 7, 2018; revised October 28, 2018; accepted April 20, 2019. This work was supported by the Enterprise Partnership Scheme of the Irish Research Council and by Analog Devices Intl.

Yeny Vázquez-Gutiérrez and Richard C. Kavanagh are with the Electrical and Electronic Engineering Department, University College Cork, Cork, Ireland. (e-mail: yeny.vazquez.gutierrez@umail.ucc.ie; r.kavanagh@ucc.ie).

Dara L. O'Sullivan is with Analog Devices, Cork, Ireland (e-mail: dara.osullivan@analog.com).

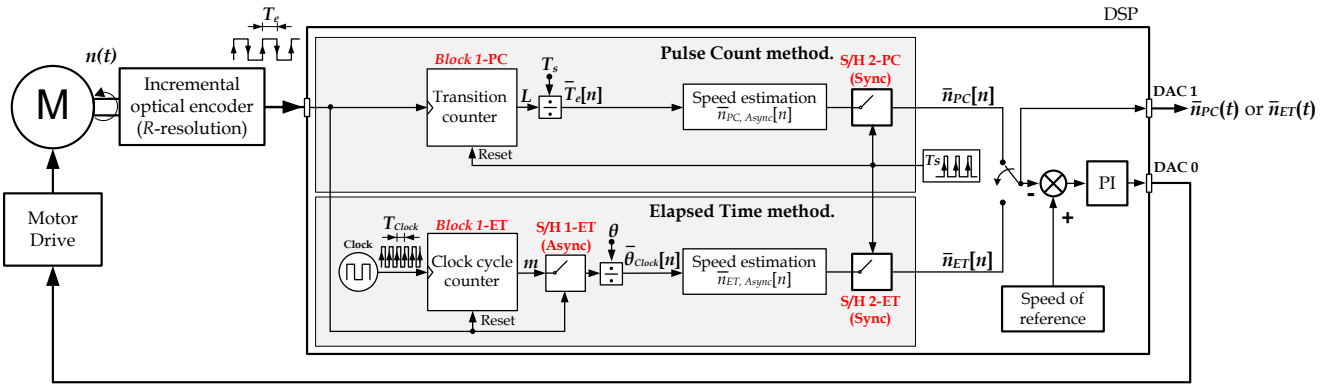

Fig. 1 Abstract representation of the encoder and the motor control system for derivation of the small-signal models.

small-signal models of incremental optical encoders over the full speed range (defined in Section II). The developed models allow an accurate prediction of the frequency response, both in magnitude and phase, of the optical encoder at different speeds. Additional effects are included in the developed small-signal models relative to those previously considered in the state of the art. The small-signal technique, frequently used in power converters [25], is applied to the encoder analysis. This paper also contributes to the experimental validation of the derived models. A practical control design case exemplifies the relevance of the developed model when the motor operates at low speed and with a low-resolution encoder. The model assists the designer in the implementation of a simple compensation technique (lead compensator) that, combined with a PI controller significantly improves the performance of the motor system at low speed.

This paper is structured in five sections. Section II covers the mathematical derivation of the new small-signal models of the two most commonly used speed estimation methods. These are: the pulse count (PC) method and the elapsed time (ET) method, both described in [11]. Section III provides the experimental validations. In Section IV, a practical use of the small- signal model for low speed control design is presented. Finally, section V presents the conclusions.

II. The Small-Signal Model of the Incremental Optical Encoder.

Table 1 defines the variables and symbols used in this paper.

The performance of the incremental optical encoder is defined by its resolution and is well described in [2]. The output of the sensor typically has two channels, nominally shifted 90° to each other, allowing the detection of the direction of the rotation, while quadrature detection, whereby all encoder transitions are counted maximizes the effective encoder resolution, R, with units of pulse per revolution (ppr).

Fig. 1 shows the simplified diagram of a closed-loop system composed mainly by the motor, driver, incremental optical encoder and the digital signal processor (DSP) where a PI controller is implemented. The small-signal models derived include the hardware and software time delays during the processes of measurement, speed estimation and update of the speed value. The models neglect the delay due to DSP calculation and DSP peripheral update-time delay because they operate at a very high frequency (usually tens of MHz).

The PC method is based on the number of encoder transitions (L) occurring over a fixed time interval (T_s). The ET method is based on the time duration (T_e) between

TABLE I
List of Symbols

Symbol	Definition
R	Effective resolution of the encoder, one, two or four (termed quadrature detection) times the number of slits nominally evenly distributed around the disc; (pulses per revolution; ppr).
θ	The minimum rotated angle detected by the sensor. $\theta = 360°/R$; degrees.
T_s	Control-loop sample time in seconds (s).
T_e	Time elapsed between consecutive encoder transitions (or edges) $T_e = 60 / (\bar{n} \cdot R)$; (s).
$n(t)$	Actual motor speed in revolutions per minute (r/min)
$\bar{n}(t)$, $\bar{n}$	Estimated and average motor speed (r/min)
L	Number of encoder transitions (edges) per control sample time T_s.
l	Normalized speed as the number of encoder transitions per sample intervals (tr./T_s)
T_{Clock}	Fixed time duration of a cycle of the peripheral high-frequency clock.
m	Number of cycles of the high-frequency clock occurring over time T_e.
θ_{Clock}	Rotated angle during a T_e period of time, $\theta_{Clock} = \theta/m$ in degrees.
t_d	Time delay (s)
$\bar{x}$	Symbolizes the average value of a signal x.
$\tilde{x}$	Symbolizes small-signal disturbance superimposed to a signal x.
f_{Enc}	Frequency of the signal of the encoder in Hz. Note that $f_{Enc} = n(t) \cdot 60 / R$
f_{VCO}	Frequency at the output of the VCO
f_o	Steady-state frequency that is modulated in the VCO; (Hz).
G	Gain of the VCO; (Hz/V)
$V_{in}(t)$	Modulator input of the VCO; (V)
k,i	Sample number indeces in the discrete domain.
$\langle x \rangle$	Symbolizes fractional part of a real number x
$\lfloor x \rfloor$	Symbolizes the floor function of a real number x
$\lceil x \rceil$	Symbolizes the ceiling function of a real number x

consecutive transitions of the encoder. A transition occurs when the motor rotates θ degrees, corresponding to the resolution R of the encoder.

The full speed range is classified in three intervals: low, medium, and high speed according to the normalized speed l

$$l = \frac{\bar{n} \cdot \frac{R}{60}}{1/T_s} \tag{1}$$

where $\bar{n}$ is the average speed.

- Low speed is defined as $l < 1$ tr./T_s, i.e. less than one encoder transition per sample time.
- This paper considers medium speed for 1 tr./$T_s \le l <$ 20 tr./T_s. In general, the criterion to delimit medium and high speed is not unique and will be application-dependent.
- High speed is hence defined for $l >$ 20 tr./T_s.

The PC method can be used, in theory, for any speed such that $l \ge 1$ tr./T_s. However, in practice it is used at high speed because of the impact of the quantization error in the control loop. For example, 20 tr./T_s implies a 5% error in the PC based speed estimation. However, for a high-inertia load this would not cause a major inconvenience because the mechanical pole filters the noise from the estimation error.

The ET method can be used, in theory, over all speed range. The ET actually provides the best estimate of the instantaneous motor speed. In practice, its use is limited to low and medium speed[1].

The dynamic behavior of the PC method is determined by the '*Block 1*-PC' (in Fig. 1) that corresponds to the *L*- counter. This is later derived to be modeled by a moving average filter $H_{MovAvg\text{-}L}(s)$. The next block is the sample and hold (composed by an ideal sampler and a zero-order-hold) 'S/H 2-PC' with an update rate of T_s. The transfer function of the PC method is:

$$H_{Enc\ PC}(s) = \frac{\bar{n}_{PC}(s)}{n(s)} = H_{MovAvg-L}(s) \cdot H_{S/H-T_s}(s) \tag{2}$$

The ET method estimates the speed based on the measured time between two encoder consecutive transitions T_e. This method is also represented in Fig. 1. The '*Block 1*-ET' corresponds to the *m*-counter (with *m* being the number of cycles of the high-frequency clock).This is modeled by a moving average filter $H_{MovAvg\text{-}m}(s)$. Every incoming encoder transition resets, by hardware, the *m*-counter. The last value of *m* is stored and latched in a DSP register until the next incoming transition. This 'S/H 1- ET' with an update rate of T_e in Fig. 1 produces the effect of a sample and hold ($H_{S/H\text{-}T_e}(s)$). However, the output $\bar{n}_{ET}[n]$ is not updated until the next control sampling instant (T_s). This is labeled in Fig. 1 as 'S/H 2- ET' with transfer function ($H_{S/H\text{-}T_s}(s)$). The encoder transitions and the sampling control are asynchronous.

[1] Real encoders have asymmetries in the signal of each channel for electrical reasons. The ET method is sensitive to these asymmetries which downgrade the performance of the control loop at medium and high speed. This is particularly true if quadrature configuration is used.

$$H_{Enc\ ET}(s) = \frac{\bar{n}_{ET}(s)}{n(s)} = H_{MovAvg-m}(s) \cdot H_{S/H-T_e}(s) \cdot H_{S/H-T_s}(s) \tag{3}$$

The transfer functions, (2) and (3), are derived in the next sub-sections A and B. In general, for the small-signal model derivation, it is assumed that a disturbance ($\tilde{x}(t)$) is superimposed on an operating point *X*.

$$x(t) = X + \tilde{x}(t) \tag{4}$$

The amplitude of the disturbance signal is much smaller than the steady-state speed value, i.e. $|X| \gg |\tilde{x}(t)|$, as in [26], so that the system nonlinearities can be neglected.

A. *The small-signal model of the pulse count method.*

The PC method is represented in Fig. 2. An ideal encoder, without mechanical or electronic nonidealities, is assumed.

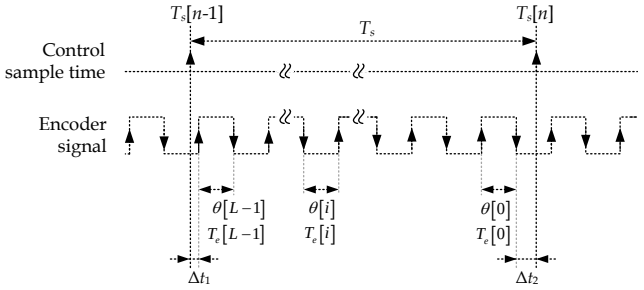

Fig. 2 The PC speed estimation method.

The speed $\bar{n}_{PC}$ is updated at regular T_s. The number of encoder transitions, *L*, per sample, varies in proportion to the speed. The rotated angle θ during T_e remains constant and proportional to the encoder resolution $\theta = 360^o/R$. The average estimated speed in r/min over interval T_s, is

$$\bar{n}_{PC} = \frac{L \cdot \theta}{T_s} \cdot \frac{60}{360} = \frac{L}{T_s} \cdot \frac{60}{R} \tag{5}$$

The fixed control sampling time T_s in (5) can be expressed as:

$$T_s \approx T_e[0] + T_e[1] + ... + T_e[i] + ... + T_e[L-1] \tag{6}$$

The average estimated speed, before the sample and hold 'S/H 2-PC' in Fig.1, can be expressed as:

$$\bar{n}_{PC\ Async}[n] = \frac{1}{\frac{T_e[0] + T_e[1] + ... + T_e[i] + ... + T_e[L-1]}{L}} \cdot \frac{60}{R} \tag{7}$$

where the speed is inversely proportional to the average $\bar{T}_e[n]$.

$$\bar{T}_e[n] = \sum_{n=0}^{L-1} \frac{T_e[n]}{L} \tag{8}$$

It has been reported in [27] that any pulse counter can be modeled as a finite -impulse-response (FIR) filter. This can be obtained from the discretization of equation (8) by applying the unilateral z-transform.

$$\frac{\bar{T}_e[z]}{T_e[z]} = \frac{1}{L} \cdot \sum_{k=0}^{L-1} z^{-k} = \frac{1}{L} \cdot \frac{1 - z^{-L}}{1 - z^{-1}} \tag{9}$$

This derivation assumes that the amplitude of the superimposed disturbance on the speed operating point does not excite non-linearities. It is demonstrated in Appendix A that small-signal properties apply also to the signal T_e.

Consequently, the time between transitions $T_e[i]$ equals to $\overline{T}_e$. The expression (9) can be mapped to the *s*-domain using the conversion factor: $z = e^{s\cdot\overline{T}_e}$ where $\overline{T}_e = T_s / L$.

$$H_{Mov\,Avg}(s) = \frac{\overline{T}_e(s)}{T_e(s)} = \frac{1}{L}\cdot\frac{1-\left(e^{s\cdot\frac{T_s}{L}}\right)^{-L}}{1-\left(e^{s\cdot\frac{T_s}{L}}\right)^{-1}} \tag{10}$$

The expression (10) is a moving average filter derived from the denominator of $\overline{n}_{PC\,Async}[n]$ that is finally located in the numerator of (2). This is mathematically justified by first considering the instantaneous input speed as:

$$n[i] = \frac{\theta[i]}{T_e[i]}\cdot\frac{60}{360} \tag{11}$$

whose small-signal expression is:

$$\tilde{n}(s) = -\frac{60/R}{T_e^{\,2}}\cdot\tilde{T}_e(s) \tag{12}$$

Similarly, the small-signal expression of the output speed in (7) is

$$\tilde{\overline{n}}_{PC\,Async}(s) = -\frac{60/R}{\overline{T}_e^{\,2}}\cdot\tilde{\overline{T}}_e(s) \tag{13}$$

Then, using $\tilde{\overline{T}}_e(s)$ as the disturbed $\overline{T}_e(s)$ and $\overline{T}_e^{\,2} = T_e^{\,2}$

$$\frac{\tilde{\overline{n}}_{PC\,Async}(s)}{\tilde{n}(s)} = \frac{-\frac{60/R}{\overline{T}_e^{\,2}}\cdot\tilde{\overline{T}}_e(s)}{-\frac{60/R}{T_e^{\,2}}\cdot\tilde{T}_e(s)} = \frac{\tilde{\overline{T}}_e(s)}{\tilde{T}_e(s)} = H_{Mov\,Avg}(s) \tag{14}$$

In steady state conditions the varying times Δt_1 and Δt_2, from Fig. 2, cause an error in the speed measurement. In the particular case of Δt_2 it produces an additional time delay that must be added to $H_{Mov\,Avg}(s)$ in (10) to correct the effects of the asynchrony between the encoder transitions and the control sample time. The phase lag due to Δt_2 varies as a sawtooth and is modeled as $e^{-T_s\cdot s/(2L)}$. This leads to the encoder transfer function of the PC method shown in (2)

$$H_{Enc\,PC}(s) = \underbrace{\frac{1}{L}\cdot\frac{1-\left(e^{s\cdot\frac{T_s}{L}}\right)^{-L}}{1-\left(e^{s\cdot\frac{T_s}{L}}\right)^{-1}}\cdot e^{-s\cdot\frac{T_s}{2L}}}_{H_{Mov\,Avg-L}(s)}\cdot\underbrace{\frac{1-e^{-s\cdot T_s}}{s\cdot T_s}}_{H_{S/H-T_s}(s)} \tag{15}$$

The same conclusion about the phase lag is achieved assuming that L is a real number instead of integer, as shown in Appendix B. This transfer function is valid for any $L \geq 1$. In practice, expression (15) can be simplified by taking the limit as L tends to ∞ for $L \geq 10$; this yields a simplified transfer function:

$$H_{Enc\,PC-Simp.}(s) = \left(\frac{1-e^{-s\cdot T_s}}{s\cdot T_s}\right)^2 \tag{16}$$

On the other hand, the same conclusion as (16) is achieved by comparing and analyzing the delay graphically for a small-signal sinusoidal disturbance, as in Fig. 3.

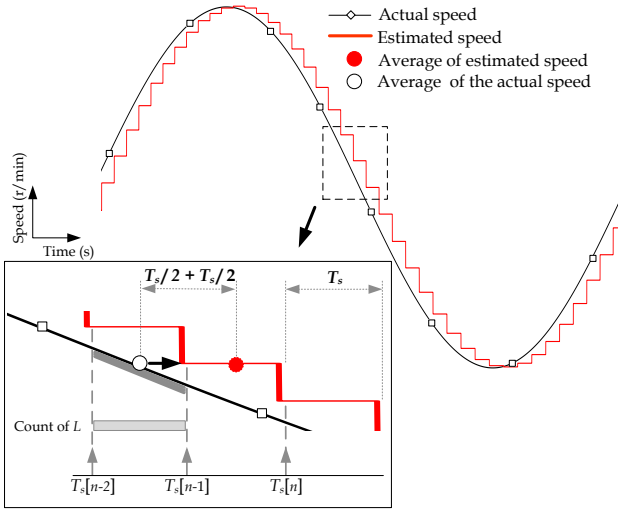

Fig. 3 Time domain representation of the average total delay of the PC speed estimation method.

During the first control sample (between $T_s[n\text{-}2]$ and $T_s[n\text{-}1]$) the DSP peripheral counts encoder transitions, L. During the subsequent control interval, the speed is calculated and held until new measured data is available, giving a total average delay of T_s, as described in (16).

B. The small-signal model of the elapsed time method.

Fig. 4 depicts a diagram of the ET method which is based on counting high-frequency clock cycles (T_{Clock}) during the time interval T_e. The rotated angle during an entire clock cycle is θ_{Clock}. The time Δt_1 corresponds to the time between an encoder transition and the next clock cycle. The time Δt_2 corresponds to the time between the last clock cycle and the encoder transition that resets the *m*-counter, with rising and falling edges. The time between the last encoder transition and the next sampling control instant is t_d. The clock is asynchronous with the encoder signal and with the control sampling interval. The average speed over the time T_e is expressed as:

$$\overline{n}_{ET} = \frac{\theta}{T_e}\cdot\frac{60}{360} \tag{17}$$

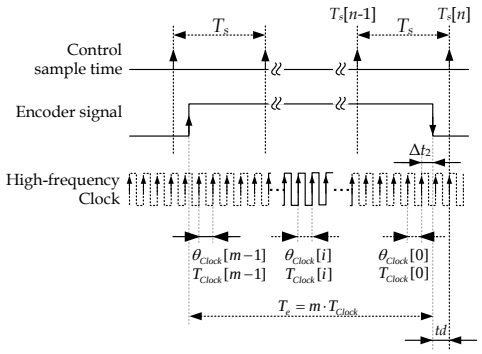

Fig. 4 The ET speed estimation method.

The time duration of the transition T_e is

$$T_e = \sum_{i=0}^{m-1} T_{Clock\,i} = m \cdot T_{Clock} \tag{18}$$

The asynchronous process leads to an error of ± 1 cycle count that in practice has little impact, given the high clock frequencies of modern DSPs.

The rotated angle θ during T_e can be obtained by considering the rotated angle over T_{Clock}.

$$\theta = \theta_{Clock}[0] + ... + \theta_{Clock}[i] + ... + \theta_{Clock}[m-1] \tag{19}$$

Then, the average speed at the instant $T_s[n]$ can be expressed as:

$$\bar{n}_{ET}[n] = \frac{\theta_{Clock}[0] + ... + \theta_{Clock}[i] + ... + \theta_{Clock}[m-1]}{m \cdot T_{Clock}} \cdot \frac{60}{360^o} \tag{20}$$

This is simplified to

$$\bar{n}_{ET} = \bar{\theta}_{Clock} \cdot \frac{60}{T_{Clock} \cdot 360^o} \tag{21}$$

where $\bar{\theta}_{Clock}$ is the average value of the rotated angle during T_{Clock}. This gives:

$$\frac{\bar{\theta}_{Clock}[z]}{\theta_{Clock}[z]} = \frac{1}{m} \cdot \sum_{k=0}^{m-1} z^{-k} = \frac{1}{m} \cdot \frac{1 - z^{-m}}{1 - z^{-1}} \tag{22}$$

Expression (22) can be mapped onto the *s*-plane by defining: $z = e^{s \cdot T_{Clock}}$ and $T_{Clock} = T_e/m$. A similar correction to the moving average in the PC method is applied to the ET method because of the delay between the consecutive transitions T_e and T_{Clock} (Δt_2) in Fig. 4. However, because m is sufficiently large over the full speed range, a limit-based simplification is always valid.

$$H_{Mov\,Avg-m}(s) = \lim_{m \to \infty} \left(\frac{1}{m} \cdot \frac{1 - \left(e^{s \cdot \frac{T_e}{m}} \right)^{-m}}{1 - \left(e^{s \cdot \frac{T_e}{m}} \right)^{-1}} \cdot \underbrace{e^{-s \cdot \frac{T_e}{2m}}}_{Correction} \right) = \frac{1 - e^{-s \cdot T_e}}{s \cdot T_e} \tag{23}$$

Because the encoder transitions and the control sampling interval are asynchronous processes, the two signals drift from each other. At constant speed, the time delay t_d between the events produced each signals is almost periodic. The delay t_d is found to vary quasi-uniformly over the period, with an average delay of $T_s/2$, as shown in Fig. 5.

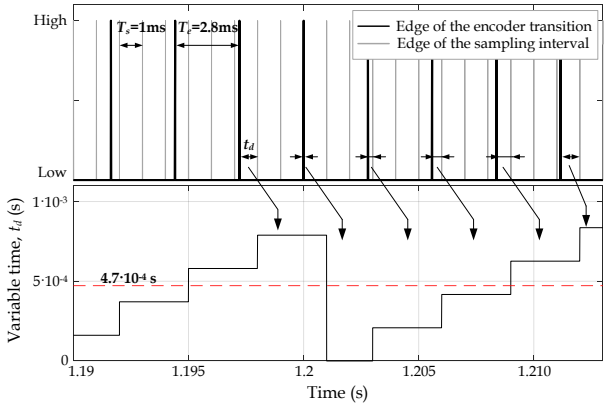

Fig. 5 Evolution of the delay t_d in the time domain with T_s = 1 ms.

This time delay is already included in the transfer function of the 'S/H 2- ET'. Then, the encoder transfer function for the ET method in (3) is:

$$H_{Enc\,ET}(s) = \underbrace{\frac{1 - e^{-s \cdot T_e}}{s \cdot T_e}}_{H_{MovAvg-m}(s)} \cdot \underbrace{\frac{1 - e^{-s \cdot T_e}}{s \cdot T_e}}_{H_{S/H-T_e}(s)} \cdot \underbrace{\frac{1 - e^{-s \cdot T_s}}{s \cdot T_s}}_{H_{S/H-T_s}(s)} \tag{24}$$

where $T_e = 60/(\bar{n}_{ET} \cdot R)$. Therefore, the encoder transfer function depends on both the resolution and the operating speed. The total average delay presented in (24) is $T_e + T_s/2$.

The conclusions presented in this paper regarding the average delay can be verified if the problem is graphically analyzed, as in Fig. 6.

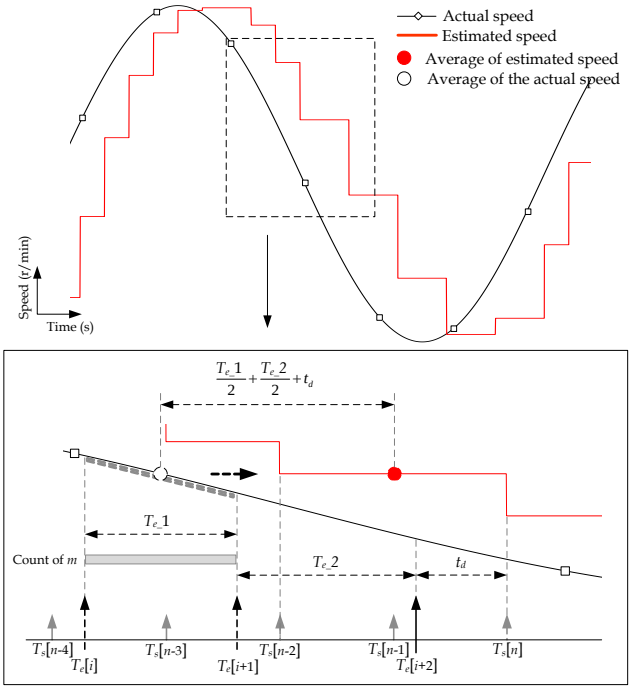

Fig. 6 Time domain representation of the average total delay of the ET speed estimation method.

Because of the small-signal analysis, it is assumed that $T_e\_1 \approx T_e\_2 \approx \bar{T}_e$, as shown in Fig. 6. The first delay corresponds to the process of counting the clock cycles during T_e_1. The second delay, from Fig. 1, models the 'S/H-1 ET'. This corresponds to the time interval over which the DSP register holds the value m. Finally, the third variable delay corresponds to the time between the encoder transition and the most immediate sampling instant that updates the value of the speed $\bar{n}_{ET}(t)$.

III. Experimental Validation of the Small-Signal Models.

The encoder is experimentally simulated with a voltage-controlled-oscillator (VCO). The VCO was previously used for PLL-based speed estimation techniques [28] to mimic the encoder. The VCO of a TG550 Function Generator modulates the frequency in proportion to the input voltage. Likewise the encoder modifies the frequency of its signal in proportion to variations in the motor speed. The output frequency of the encoder is:

$$f_{Enc}(t) = R \cdot (\bar{n} + \tilde{n}(t)) / 60 \tag{25}$$

and similarly the frequency of the VCO is:

$$f_{VCO}(t) = f_o + G \cdot V_{in}(t) \quad (26)$$

with G being the gain (Volts/Hz) of the VCO. The steady state speed is set by $\bar{n} = f_o \cdot 60 / R$; the small-signal disturbance is set by $\tilde{n}(t) = V_{in}(t) \cdot G \cdot 60 / R$, as depicted in Fig. 7.

In Fig. 7, the Analog Discovery, as network analyzer, introduces a disturbance of small amplitude $V_{in}(t)$. The VCO produces a squarewave of variable frequency, as in (26). The DSP peripheral, that processes the encoder signal, is the general purpose counter (CNT). The peripheral provides information on the number of transitions (L) and the time between pulses (T_e) for estimating the speed. The speed is digitally computed and transformed into an analog signal by a digital to analog converter (DAC) with a high update frequency that does not affect the experiment. Measurement by the Analog Discovery unit compares the input and output to measure the frequency response of the encoder. It is important to check that the configuration of the peripherals does not introduce additional unknown delays in the measurement.

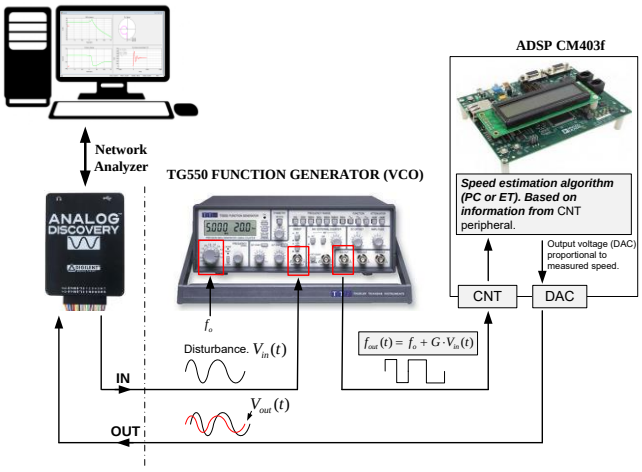

Fig. 7 Setup for the experimental validation of the models.

The experimental tests validate the developed small-signal models and compare the results with existing models.

A. *Medium and high speeds* (≥1tr./T_s).

The model for the PC method found in [23] is:

$$H_{Literature\ PC}(s) = e^{-s \cdot \frac{T_s}{2}} \quad (27)$$

Fig. 8 shows the experimental results for the PC method at a speed of 3600 r/min (30 tr./T_s). This result validates the proposed model for the PC-based method, as a moving average filter and an additional S/H. The accurate modeling of the PC-method is a major contribution of the present work, utilizing the small-signal methodology. The noise below 500 Hz is due to encoder quantization, while that above 500 Hz is due to aliasing, given the 1 ms sample interval.

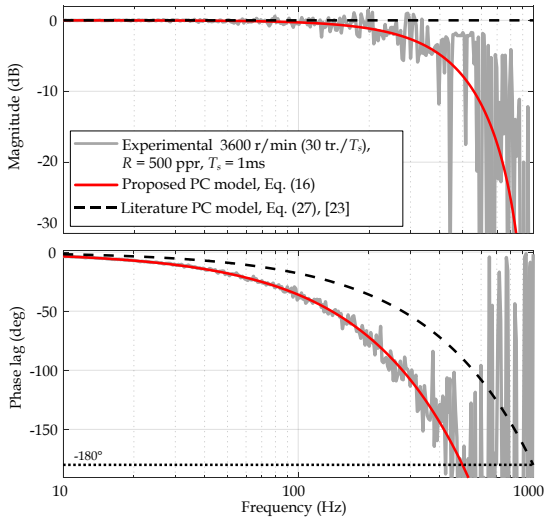

Fig. 8 Experimental validation and comparison of the PC models.

The experimental validation of the small-signal model of the ET method is shown in Fig. 9 for 3600 r/min, which is sampled at 0.1 ms and the nominal speed is 3 tr./T_s

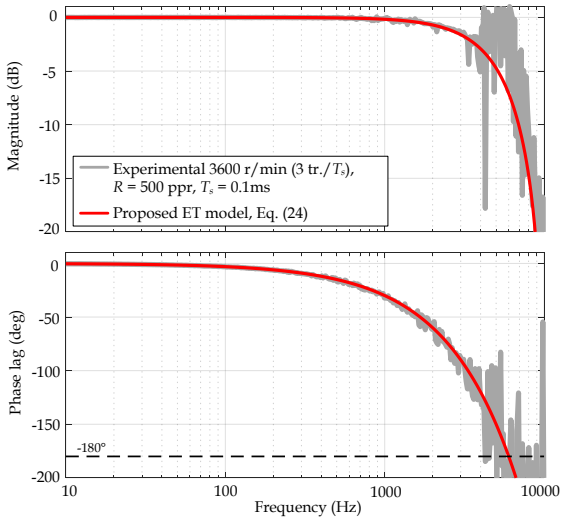

Fig. 9 Experimental validation of the ET small-signal model at medium speed.

Fig. 10 shows the experimental results for the ET method at a speed of 3600 r/min (30 tr./T_s). The proposed transfer function for the ET method in (24) is also validated for high speeds. It is observed that this method is not affected by quantization error and has a smaller phase lag than the PC method.

The speed is estimated based on the most recent encoder transition. Consequently, the resulting value does not average over L transitions, unlike the PC method. However, the ET method is more sensitive to encoder mechanical and electric nonidealities, affecting the control loop adversely. Therefore, its use is not practical for very high speeds.

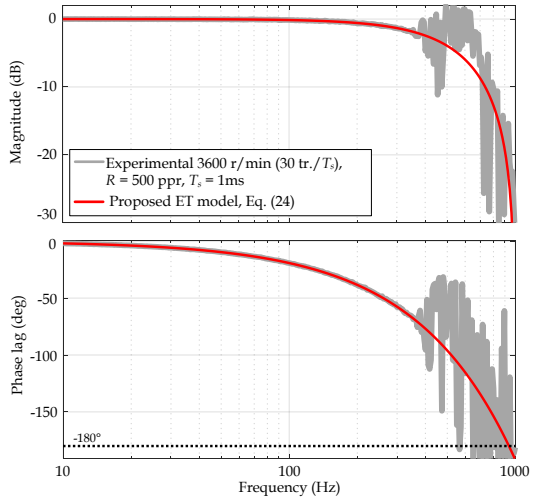

Fig. 10 Experimental validation of the ET small-signal model at high speed.

B. *Low speed* (<1 tr./T_s).

The following model is proposed in [23] for the ET method

$$H_{Literature\,ET-1}(s) = e^{-s\cdot T_e} \tag{28}$$

An alternative model is found in [24]

$$H_{Literature\,ET-2}(s) = \frac{1-e^{-s\cdot T_e}}{s\cdot T_e} \tag{29}$$

Fig. 11 shows the experimental results for the ET method at low speed 100 r/min, at two different sampling times of 1 ms (Case A) and 0.1 ms (Case B), with normalized speed of 0.83 tr./T_s and 0.083 tr./T_s, respectively.

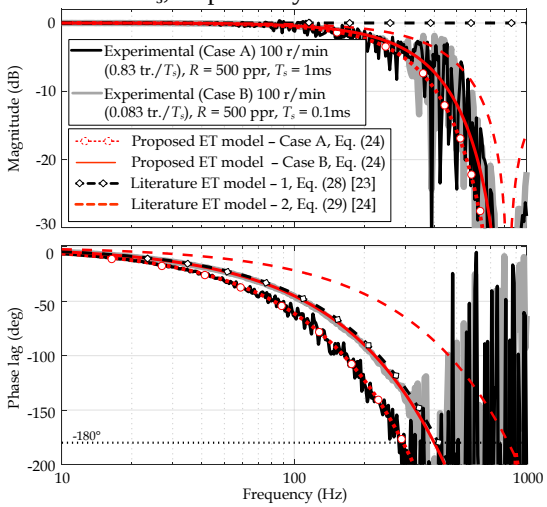

Fig. 11 Experimental validation and comparison of the ET small-signal models at two different sample times, at low speed.

The proposed model for the ET method is validated for all test conditions. It is also observed that the "Literature ET model – 1" (in Fig. 11) has unity gain and fits the phase lag of Case B because $T_e \gg T_s$, so the predominant phase lag is produced by the encoder signal.

Similarly to the PC method, the accurate ET model is a key contribution in this work.

Overall, the small-signal model of the PC method is valid for medium and high speed and the small-signal model of the ET method is valid for all speed ranges, regardless of the technical constraints imposed by real encoders.

IV. Practical Use of the Proposed Model.

The performance of the motor system deteriorates as the speed and the encoder resolution are reduced, due to the negative impact of the encoder phase lag on the control-loop. This section presents a procedure to overcome this issue. The small-signal model corresponding to the ET speed estimation method (24) is used to predict the stability and compensate the incorrect performance motor system at such conditions by means of a lead compensator. This procedure is experimentally tested in the workbench depicted in Fig. 12-(a), which is structured as shown in Fig. 12-(b). The block diagram of the resulting compensated system is depicted in Fig. 12-(c).

The system in Fig. 12-(a) is composed of a DC power supply, a DC motor, an incremental optical encoder, a linear motor drive, and an external DSP. The motor drive receives as an input a voltage command from the speed compensator implemented in the DSP. The duty cycle of the output of the motor drive is proportional to the voltage applied to the input of the same device. The output of the PI is transformed into an analog signal by the DAC (maximum output voltage: 2.5 V). An analog amplifier circuit, K in Fig. 12-(a), has been added to interface between the DAC and the input of the linear motor driver (maximum input voltage of the motor driver: 10 V).

The ET method is used to estimate the speed based on the number of m counted by the CNT peripheral:

$$\bar{n}_{ET} = \frac{1}{m\cdot T_{Clock}}\cdot\frac{60}{R} \tag{30}$$

A PI compensator is used to regulate the speed. The PI has been tuned to illustrate the impact of the encoder dynamics at low speed, as well as the usefulness of the proposed model to predict stability issues. Specifically, the gains of the PI controller are adjusted based on the frequency response of the plant within the speed loop, in a way that the system is stable at 500 r/min (where the impact of the encoder dynamics is negligible) but unstable at 15 r/min (where the impact of the encoder dynamics is significant on the phase).

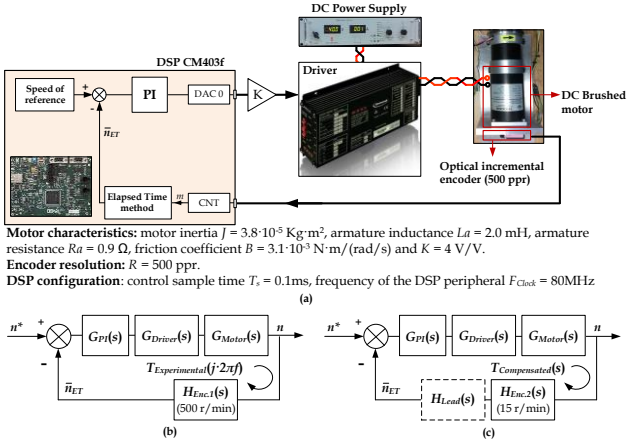

Motor characteristics: motor inertia J = 3.8·10⁻⁵ Kg·m², armature inductance La = 2.0 mH, armature resistance Ra = 0.9 Ω, friction coefficient B = 3.1·10⁻³ N·m/(rad/s) and K = 4 V/V.
Encoder resolution: R = 500 ppr.
DSP configuration: control sample time T_s = 0.1ms, frequency of the DSP peripheral F_{Clock} = 80MHz

Fig. 12 (a) Diagram of the dc motor system, (b) block diagram of the system and (c) compensated block diagram.

The first step consists of the measurement of the open-loop transfer function $T_{Experimental}(j2\pi f)$ at a speed of 500 r/min (0.42 tr./T_s) with an encoder of 500 ppr, as shown in Fig. 13. The experimental result is fitted up to 20 Hz.

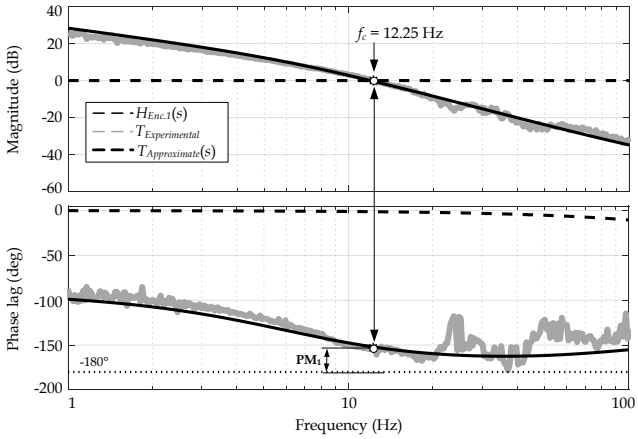

Fig. 13 Experimental frequency response of the loop gain of the dc motor system at 500 r/min (0.42 tr./T_s)

The polynomial that fits the experimental results is depicted in Fig. 13 as $T_{Approximation}(s)$. The crossover frequency f_c is 12.25 Hz. The phase margin PM_1 = 28.43° confirms the stability of the system. At this speed, the encoder $H_{Enc.1}(s)$, based on equation (24), has no impact on the overall dynamics below f_c.

The small-signal model for the ET method (24) predicts the PM at any speed. The theoretical speed limit is 19.9 r/min in the system under study, as the performance degrades below this value.

The open-loop transfer function of the system at a lower speed of 15 r/min (0.0125 tr./T_s) is analytically obtained as

$$T(s) = T_{Approximation}(s) \cdot H_{Enc\,2}(s) \tag{31}$$

where the corresponding transfer function of the encoder is $H_{Enc.2}(s)$. The resulting transfer function[2] is depicted in Fig. 14.

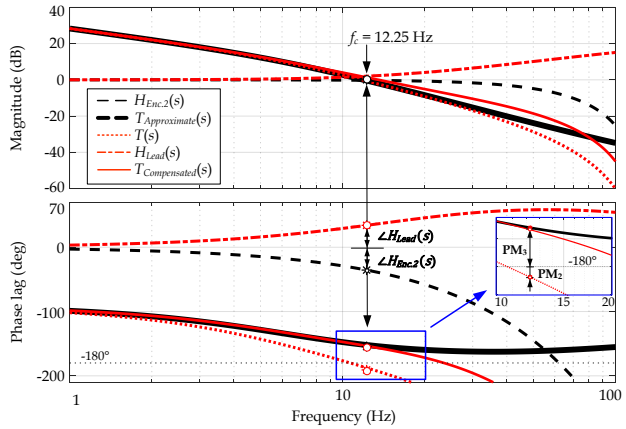

Fig. 14 Loop gain frequency response of the dc motor system at 15 r/min (0.0125 tr./T_s) with and without compensation.

At the speed of 15 r/min the system oscillates around the target speed, as observed in Fig. 15-(a) due to the phase margin PM_2 = -8.54° shown in Fig. 14. A lead compensator [26] is used in in the feedback loop, as shown in Fig. 12 (c).

$$T_{Compensated}(s) = T(s) \cdot H_{Lead}(s) \tag{32}$$

The lead compensator boosts the phase margin to PM_3 = 25.5°, as depicted in Fig. 14. Consequently, the speed tracking performance is significantly improved, as can be seen in Fig. 15-(b).

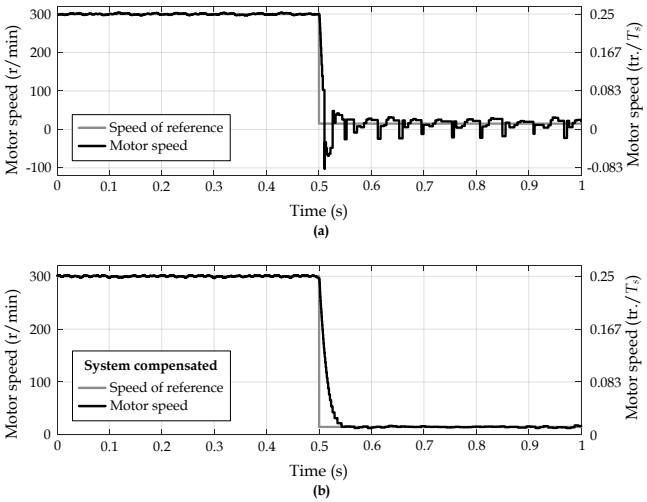

Fig. 15 Speed test response from 300 r/min (0.25 tr./T_s) to 15 r/min (0.0125 tr./T_s) where (a) is uncompensated closed-loop system and (b) the compensated closed-loop system.

The equation of the compensator is:

$$H_{Lead}(s) = \frac{1 + s \cdot T_e/\alpha}{1 + s \cdot T_e/\beta} = \frac{\beta}{\alpha} \cdot \frac{\alpha/T_e + s}{\beta/T_e + s} \tag{33}$$

The zero and the pole are placed as a function of the speed of reference proportional to T_e=60 / ($R \cdot n$*). In this example (representing a typical application) the coefficients α and β are fixed to the values of 0.8 and 10, respectively. In Fig. 14, $\angle H_{Lead}(j2\pi f)$ = 34.06°, $\angle H_{Enc.2}(j2\pi f)$ = -35.5°. The drawback of a lead compensator is the magnification of noise. However, at low speed, the ET method exhibits a very low speed error ($1/m$). Moreover, the attenuation of the loop balances any augmentation made by the lead compensator.

Through this section, a controller with constant parameter has been used. If desired, the developed small-signal models could be used to design adaptive control methods, so that the control parameters are modified depending on the operating speed.

V. Conclusion

The newly derived small-signal models of the incremental optical encoder for the PC and ET speed estimation methods are experimentally validated. The models quantify the negative impact of the phase lag of the sensor on the phase margin of the control loop. It is demonstrated that the sensor (software and hardware) attenuates the value of the speed at high frequencies. The phase lag of the sensor is determined by the fixed control sample time at high speeds (PC method). Conversely, the small-signal model of the encoder depends of the resolution of the sensor and the motor speed at low speed (ET method). The phase lag of the sensor reduces the phase

[2] Note that the delay $H_{S/H\text{-}Ts}(s)$ in the expression (23) is implicit in the experimental data, so this term should not be included in $H_{Enc.2}(s)$ for this analysis.

margin of the controller. The simplified small-signal model for the ET method is successfully used to implement a simple control technique based on a lead compensator. This technique provides a phase lead that compensates for the phase lag introduced by the speed sensor and recovers the system stability at low speed and when using a low-resolution encoder. The derived small-signal models, that combine both the encoder sensor and the speed estimation methods, assist in the design of a simple motor control technique for incremental optical encoder-based controllers.

APPENDIX A

It is stated that $|\ \bar{n}\ | \gg |\tilde{n}(t)| \Leftrightarrow |\ \bar{T}_e\ | \gg |\tilde{T}_e(t)|$. The instantaneous speed is expressed as:

$$n(t) = \bar{n} + \tilde{n}(t) = \frac{1}{T_e(t)} \cdot \frac{60}{R} = \frac{1}{\bar{T}_e + \tilde{T}_e(t)} \cdot \frac{60}{R} \tag{34}$$

The variable term in (34) is expanded as a Taylor and Maclaurin series:

$$\frac{1}{\bar{T}_e + \tilde{T}_e(t)} = \frac{1}{\bar{T}_e} - \frac{\tilde{T}_e(t)}{\bar{T}_e^2} + \frac{\tilde{T}_e(t)^2}{\bar{T}_e^3} - \frac{\tilde{T}_e(t)^3}{\bar{T}_e^4} + \ldots \tag{35}$$

Considering that$|\ \bar{T}_e\ | \gg |\ \tilde{T}_e\ |$ the third and the higher order terms in (35) can be neglected and the speed expressed as:

$$n(t) = \bar{n} + \tilde{n}(t) = \left(\frac{1}{\bar{T}_e} - \frac{\tilde{T}_e(t)}{\bar{T}_e^2} \right) \cdot \frac{60}{R} \tag{36}$$

where $\bar{n} = \left(60/R\right)/\bar{T}_e$ and $\tilde{n}(t) = -\left(60/R\right) \cdot \tilde{T}_e(t)/\bar{T}_e^2$. Finally,

$$\frac{|\tilde{n}(t)|}{|\bar{n}|} = \frac{\left| -\frac{\tilde{T}_e(t)}{\bar{T}_e^2} \cdot \frac{60}{R} \right|}{\left| \frac{1}{\bar{T}_e} \cdot \frac{60}{R} \right|} = \frac{|\tilde{T}_e(t)|}{|\bar{T}_e|} \tag{37}$$

Variations in T_e are proportional to the introduced speed disturbance, so T_e is quasi-invariant and equal to $\bar{T}_e$.

APPENDIX B

Even at constant velocity, where the average value of L over several samples is the real number $\bar{L}$, the integer number of transitions will vary by one from cycle to cycle, in an almost periodic sequence. The output will be $\lfloor \bar{L} \rfloor$, where $\lfloor \cdot \rfloor$ is the floor function of $\bar{L}$, with probability $1-\langle \bar{L} \rangle$, and $\lceil \bar{L} \rceil = \lfloor \bar{L} \rfloor + 1$, (the 'ceiling function'), with probability $\langle \bar{L} \rangle$. Note that the fractional part of $\bar{L}$ is $\langle \cdot \rangle$. The PC method implicitly differentiates the quantized shaft position estimate, with considerable mean-squared error, but zero average error, even when the encoder is not ideal [29]. Note that $\bar{L} = \lceil \bar{L} \rceil \cdot \langle \bar{L} \rangle + \lfloor \bar{L} \rfloor \cdot \left(1 - \langle \bar{L} \rangle\right)$, indicating zero average velocity error in steady state. If the actual real velocity in steady-state is $\bar{L}$ tr./T_s, the distinction between those samples for which the PC output gives estimates of $\lfloor \bar{L} \rfloor$ and $\lceil \bar{L} \rceil$ is dependent on the time delay since the encoder transition just before the sampling instant. This delay, shown in Fig. 2, exhibits almost periodic variation; thereby introducing a delay-type noise into the system, on a sample-by-sample basis. Explicitly, those samples for which the velocity estimate is $\lceil \bar{L} \rceil$ occurs when $0 \le \Delta t_2 < \langle \bar{L} \rangle T_S / \bar{L}$. This is governed by a uniform distribution and has a probability of $\langle \bar{L} \rangle$, with an average delay of $\langle \bar{L} \rangle T_S / 2\bar{L}$ .The corresponding average delay of the most delayed edge, delayed by a further $\lfloor \bar{L} \rfloor$ transitions, is $(\langle \bar{L} \rangle / (2\bar{L}) + \lfloor \bar{L} \rfloor / \bar{L}) \cdot T_S$, giving an average delay in this case of $(\langle \bar{L} \rangle / (2\bar{L}) + (\lfloor \bar{L} \rfloor / 2) / \bar{L}) \cdot T_S = T_S / 2$ to the transition instants. However the fact that the speed estimate is constant over $Ts / \bar{L}$ implies total average delay of $T_S / 2 + T_S / (2\bar{L})$ Similarly, when the velocity estimate is $\lfloor \bar{L} \rfloor$, which occurs when $\langle \bar{L} \rangle T_S / \bar{L} \le \Delta t_2 < T_S / \bar{L}$, the average delay can again be shown to be $T_S / 2 + T_S / (2\bar{L})$. Therefore, the statistical analysis shows that the average delay of the PC method is $T_S / 2 + T_S / (2\bar{L})$. Combined with the delay of the 'S/H-1PC', this gives an overall delay of $T_S + T_S / (2\bar{L})$. The variation of the sample-by-sample delays clearly indicates that use of the small-signal model is suitable for the analysis of the encoder-based system, and that the actual system will contain increasingly significant noise as L decreases in the PC method, due to the quantized nature of the sensor.

REFERENCES

[1] M. Zhao and J. Lin, "Health Assessment of Rotating Machinery Using a Rotary Encoder," *IEEE Trans. Ind. Electron.*, vol. 65, no. 3, pp. 2548–2556, Mar. 2018.

[2] P. P. L. Regtien, *Sensors for mechatronics*, 1st ed. Amsterdam ; New York: Elsevier, 2012.

[3] K. Saito, K. Kamiyama, T. Ohmae, and T. Matsuda, "A microprocessor-controlled speed regulator with instantaneous speed estimation for motor drives," *IEEE Trans. Ind. Electron.*, vol. 35, no. 1, pp. 95–99, Feb. 1988.

[4] C. Xia, B. Ji, and Y. Yan, "Smooth Speed Control for Low-Speed High-Torque Permanent-Magnet Synchronous Motor Using Proportional-Integral-Resonant Controller," *IEEE Trans. Ind. Electron.*, vol. 62, no. 4, pp. 2123–2134, Apr. 2015.

[5] J. Lara, J. Xu, and A. Chandra, "Effects of Rotor Position Error in the Performance of Field-Oriented-Controlled PMSM Drives for Electric Vehicle Traction Applications," *IEEE Trans. Ind. Electron.*, vol. 63, no. 8, pp. 4738–4751, Aug. 2016.

[6] P. J. Roche, J. M. D. Murphy, and M. G. Egan, "Reduction of quantisation noise in position servosystems," in *and Automation Proceedings of the 1992 International Conference on Industrial Electronics, Control, Instrumentation*, 1992, pp. 464–469 vol.1.

[7] R. Raja, T. Sebastian, M. Wang, A. Gebregergis, and M. S. Islam, "Effect of Position Sensor Error on the Performance of Permanent Magnet Machine Drives," *IEEE Trans. Ind. Appl.*, vol. 53, no. 6, pp. 5518–5526, Nov. 2017.

[8] R. Iskakov, A. Albu-Schaeffer, M. Schedl, G. Hirzinger, and V. Lopota, "Influence of sensor quantization on the control performance of robotics actuators," in *2007 IEEE/RSJ International Conference on Intelligent Robots and Systems*, 2007, pp. 1085–1092.

[9] V. Kisner, E. Lenz, A. Wahrburg, K. D. Listmann, and U. Konigorski, "Harmonic approximation of velocity oscillations in electrical drives," in *2016 IEEE Conference on Control Applications (CCA)*, 2016, pp. 1137–1142.

[10] S.-M. Yang and S.-J. Ke, "Performance evaluation of a velocity observer for accurate velocity estimation of servo motor drives," *IEEE Trans. Ind. Appl.*, vol. 36, no. 1, pp. 98–104, Jan. 2000.

[11] T. Ohmae, T. Matsuda, K. Kamiyama, and M. Tachikawa, "A Microprocessor-Controlled High-Accuracy Wide-Range Speed

Regulator for Motor Drives," *IEEE Trans. Ind. Electron.*, vol. IE-29, no. 3, pp. 207–211, Aug. 1982.

[12] R. C. Kavanagh, "An enhanced constant sample-time digital tachometer through oversampling," *Trans Inst Meas Control*, vol. 26, no. 2, pp. 83–98, Apr. 2004.

[13] H.-W. Kim and S.-K. Sul, "A new motor speed estimator using Kalman filter in low-speed range," *IEEE Trans. Ind. Electron.*, vol. 43, no. 4, pp. 498–504, Aug. 1996.

[14] A. Suzumura, Y. Fujimoto, T. Murakami, and R. Oboe, "A General Framework for Designing SISO-Based Motion Controller With Multiple Sensor Feedback," *IEEE Trans. Ind. Electron.*, vol. 63, no. 12, pp. 7607–7620, Dec. 2016.

[15] R. H. Brown, S. C. Schneider, and M. G. Mulligan, "Analysis of algorithms for velocity estimation from discrete position versus time data," *IEEE Trans. Ind. Electron.*, vol. 39, no. 1, pp. 11–19, Feb. 1992.

[16] S. Jeon, "State estimation based on kinematic models considering characteristics of sensors," in *Proceedings of the 2010 American Control Conference*, 2010, pp. 640–645.

[17] A. Anuchin, V. Astakhova, D. Shpak, A. Zharkov, and F. Briz, "Optimized method for speed estimation using incremental encoder," in *2017 International Symposium on Power Electronics (Ee)*, 2017, pp. 1–5.

[18] L. Kovudhikulrungsri and T. Koseki, "Precise Speed Estimation From a Low-Resolution Encoder by Dual-Sampling-Rate Observer," *IEEEASME Trans. Mechatron.*, vol. 11, no. 6, pp. 661–670, Dec. 2006.

[19] W. H. Chen, J. Yang, L. Guo, and S. Li, "Disturbance-Observer-Based Control and Related Methods--An Overview," *IEEE Trans. Ind. Electron.*, vol. 63, no. 2, pp. 1083–1095, Feb. 2016.

[20] S. A. A. Rizvi, M. Faisal, H. Aftab, S. Ahmed, and A. Y. Memon, "A robust observer and controller design for a DC motor with a low-resolution encoder," in *The 27th Chinese Control and Decision Conference (2015 CCDC)*, 2015, pp. 3038–3043.

[21] T.-J. Kweon and D.-S. Hyun, "High-performance speed control of electric machine using low-precision shaft encoder," *IEEE Trans. Power Electron.*, vol. 14, no. 5, pp. 838–849, Sep. 1999.

[22] T. Shi, Z. Wang, and C. Xia, "Speed Measurement Error Suppression for PMSM Control System Using Self-Adaption Kalman Observer," *IEEE Trans. Ind. Electron.*, vol. 62, no. 5, pp. 2753–2763, May 2015.

[23] R. Bonert, "Digital Tachometer with Fast Dynamic Response Implemented by a Microprocessor," *IEEE Trans. Ind. Appl.*, vol. IA-19, no. 6, pp. 1052–1056, Nov. 1983.

[24] L. Bascetta, G. Magnani, P. Rocco, and A. M. Zanchettin, "Performance Limitations in Field-Oriented Control for Asynchronous Machines With Low Resolution Position Sensing," *IEEE Trans. Control Syst. Technol.*, vol. 18, no. 3, pp. 559–573, May 2010.

[25] L. Corradini, D. Maksimović, P. Mattavelli, and R. Zane, *Digital control of high-frequency switched-mode power converters*, 1st ed. New Jersey: John Wiley & Sons, Inc., 2015.

[26] K. Ogata, *Modern control engineering*, 4. ed., international ed. Upper Saddle River, NJ: Prentice Hall [u.a.], 2002.

[27] L. Bascetta, G. Magnani, and P. Rocco, "Velocity Estimation: Assessing the Performance of Non-Model-Based Techniques," *IEEE Trans. Control Syst. Technol.*, vol. 17, no. 2, pp. 424–433, Mar. 2009.

[28] T. Emura and L. Wang, "A high-resolution interpolator for incremental encoders based on the quadrature PLL method," *IEEE Trans. Ind. Electron.*, vol. 47, no. 1, pp. 84–90, Feb. 2000.

[29] R. C. Kavanagh and J. M. D. Murphy, "The effects of quantization noise and sensor nonideality on digital differentiator-based rate measurement," *IEEE Trans. Instrum. Meas.*, vol. 47, no. 6, pp. 1457–1463, Dec. 1998.

Yeny Vázquez-Gutiérrez was born in Cuba in 1988. She received the B.E. and M.Eng.Sc. degrees in electrical engineering from the University Carlos III of Madrid, Spain, in 2011 and 2014 respectively. She is pursuing the doctoral degree in the University College Cork (UCC), Cork, Ireland.

From 2010 to 2012 she worked as undergraduate research intern in Grupo de Sistemas Electrónicos de Potencia (GSEP) in the University Carlos III of Madrid. She is currently working as power electronic engineer in Albatros Electrónica de Potencia S.L.U.

Her current research interests include motor drive, motion control for motors and auxiliary power supply design.

Dara L. O'Sullivan received his B.E, M.Eng.Sc. and Ph.D. from University College Cork (UCC), Ireland, in 1995, 1997 and 2001 respectively.

He has worked in industrial and renewable energy applications in a range of research, consultancy and industry positions since 2001. He is currently a System Applications Manager with the Connected Motion and Robotics team within the Automation & Energy business unit at Analog Devices. His area of expertise is power conversion, control and monitoring in industrial motion control applications.

Richard C. Kavanagh (M'95-SM'01) received the B.E., M.Eng.Sc and Ph.D. degrees in electrical engineering from the National University of Ireland in 1984, 1985 and 1988, respectively.

He previously worked as a Senior Research Scientist with PEI Technologies, and as a Senior Project Engineering with SPS Laboratories Ltd. He is a Senior Lecturer in Electrical and Electronic Engineering and Director of the Mechatronics Research Laboratory in the School of Engineering, University College Cork, Ireland, where he also served as Dean of Engineering from 2005-2012.

His current research interest include improved sensor and motion controller design through advanced signal processing and analysis of quantized signals, and the control of compliant mechanisms for nanopositioning application.

Dr. Kavanagh served as an Associate Editor of the IEEE Signal Processing Letters from 2002 to 2005. He is a Fellow of the Institution of Engineers of Ireland.